Arabian Journal for Science and Engineering (2019) 44:7843–7858
https://doi.org/10.1007/s13369-019-03918-3

RESEARCH ARTICLE -MECHANICAL ENGINEERING

Experimental Investigation of Machinability and Surface Characteristics in Microelectrical Discharge Milling of Titanium, Stainless Steel and Copper

Siddhartha Kar[1] · **Promod Kumar Patowari**[1]

Received: 1 March 2019 / Accepted: 13 May 2019 / Published online: 24 May 2019

Abstract
Microelectrical discharge milling (μED-milling) possesses good processing capability to fabricate intricate shapes in any electrically conductive material. In the present work, an experimental study is carried out to investigate machinability and surface characteristics of titanium (Ti) grade 2 alloy, stainless steel 304 (SS304) and copper (Cu) undergoing microelectrical discharge milling (μED-milling) process. Voltage, feed rate (FR) and tool rotation speed (TRS) are the process parameters that are varied during machining. The response measures chosen for evaluating machinability performance are material removal rate (MRR) and tool wear rate (TWR). After performing μED-milling, topography of the fabricated microslots is characterized by optical microscopy, scanning electron microscopy and surface roughness (Ra) analysis, whereas material composition analysis is carried out by X-ray diffraction and energy-dispersive X-ray techniques. It is found that Cu exhibits higher MRR than Ti and SS304, whereas SS304 exhibits higher TWR than Ti and Cu at all the chosen parametric conditions. The most significant parameter affecting MRR and TWR as ascertained by analysis of variance is FR, followed by voltage and TRS. Surface morphology of the microchannels fabricated by μED-milling reveals that globule formation and redeposition phenomenon is profound in case of Cu and SS304. In contrast, Ti grade 2 exhibits better surface morphology in terms of less globule formation, microvoids, redeposition layer and lower Ra as compared to Cu and SS304.

Keywords Micromachining · Microelectrical discharge milling · EDM · Titanium · Stainless steel · Copper

1 Introduction

Component miniaturization is the present buzzing topic trending with technological improvement in aerospace, biomedical engineering, electronics, military application, etc. The emergence of microsystems enhanced the quality of life by improving health care and economic growth, thus grabbing the attention of the commercial industries [1]. Among several manufacturing techniques that are available to fabricate miniaturized products, microelectrical discharge machining (μEDM) is a prominent and reliable process for machining hard materials which are difficult to machine by conventional machining processes [2]. μEDM has the ability to process any electrically conductive material regardless of their hardness and can generate intricate shapes with good surface finish [3, 4]. In this process, material is removed by melting and evaporation due to repetitive discharges occurring between tool and workpiece electrode which are immersed in a dielectric medium [5]. With the advent of μEDM over the years, several variants of μEDM have evolved, among which microelectrical discharge milling (μED-milling) is particularly used for machining complex three-dimensional (3D) microfeatures [6]. μED-milling can cut complex shapes with a simple cylindrical tool, and unlike sinking μEDM, it avoids manufacturing of sophisticated tool for attaining intricate 3D profiles [7]. But, it endures few limitations in the form of tool electrode wear and low machining efficiency [8]. Tool wear is an inherent phenomenon of any electrical discharge machining (EDM) variant, which results in dimensional inaccuracy that cannot be eliminated completely [9]. Researchers have conducted various studies over the years to overcome these limitations. A detailed review of the tool wear compensation strategies implemented in μED-milling has been reported by Kar and Patowari [10].

✉ Siddhartha Kar
siddkar.nita@gmail.com

[1] Department of Mechanical Engineering, National Institute of Technology Silchar, Silchar, Assam 788010, India

Table 1 Physical properties of workpiece materials

Material	Electrical resistivity (Ω-cm)	Thermal conductivity (W/m-K)	Melting temperature (°C)	Specific heat capacity (J/g-°C)
Titanium grade 2	5.2×10^{-5}	16.4	1665	0.523
Stainless steel 304	7.2×10^{-5}	16.2	1400–1450	0.5
Copper	1.7×10^{-6}	385	1083	0.385

In μEDM, the pulse energy required in the machining gap to fabricate microparts is less, as material is removed in the range of subgrain size (0.1–10 μm) [11]. Supply of such lower pulse energy can be fulfilled by the resistance capacitance (RC)-type generator [12]. Other than discharge energy, tool rotation speed (TRS), feed rate (FR), layer thickness, etc., also play vital roles in μED-milling. Mehfuz and Ali [1] found capacitance and voltage individually influence material removal rate (MRR), maximum peak-to-valley roughness height (R_y), average surface roughness (R_a) and electrode wear ratio (EWR), whereas FR influences MRR only in μED-milling of beryllium–copper (Be–Cu) workpiece with tungsten tool electrode. Karthikeyan et al. [13] examined the effect of energy, TRS, FR and aspect ratio on MRR and tool wear rate (TWR) in μED-milling of EN 24 workpiece with tungsten tool electrode. MRR and TWR increased with an increment in energy (500–2000 μJ) and TRS (100–800 rpm) but decreased in case of FR and aspect ratio exceeding 45 μm/s and 1.5, respectively. In another study, Karthikeyan et al. [14] found TRS and energy to be the most influential parameters for maximizing MRR and minimizing TWR, respectively. In simultaneous optimization of maximizing MRR and minimizing TWR, FR was found to have the maximum influence. Chiou et al. [15] investigated the effect of applying silver (Ag) and copper (Cu) coating on tungsten carbide (WC) tool electrode in μED-milling of high-speed steel alloy. The coated electrodes improved surface roughness (Ra) and MRR, wherein lowest SR and highest MRR were achieved by WC-coated Ag and WC-coated Cu electrodes, respectively. WC electrode exhibited lowest tool wear owing to its superior melting temperature as compared to Ag and Cu. Kuriachen and Mathew [16] observed that capacitance and FR were the most influencing factors in μED-milling of Ti–6Al–4V by WC tool electrode. They found a redundant effect on MRR and TWR after a certain value of voltage (115 V). In case of TRS, the rise in MRR was slow after a critical level (1000 rpm) due to the generation of unproductive sparks. A non-uniform recast layer was witnessed on the machined surface owing to the resolidification phenomenon of melted material. Kuriachen and Mathew [17] also examined the effect of SiC powder suspended in dielectric on machining of Ti–6Al–4V with WC tool electrode. Low TWR and high MRR were simultaneously attained for 5 g/L powder concentration (lowest), 0.1 μF capacitance (medium) and 115 V voltage (medium). Machined surfaces at the two ends of the microslots were exposed to microholes and microcracks due to frequent change in the temperature at the ends. Jafferson et al. [18] examined the effect of non-electrical factors such as layer thickness, FR and TRS on MRR, TWR and EWR in μED-milling of stainless steel (SS) with tungsten tool electrode. To achieve maximum MRR and minimum TWR, higher TRS of 2500 rpm and FR of 100 mm/min were recommended. Ununo and Mali [19] found an increase in MRR and decrease in frontal electrode wear with the use of low-frequency workpiece vibration while fabricating microchannels on Inconel 718 by μED-milling.

Table 2 Variable and fixed process parameters

Variable parameters with their levels		
Parameter	Level	Values
Voltage (V)	3	80, 130, 180
Feed rate (μm/s)	3	5, 12.5, 20
Tool rotation speed (rpm)	3	500, 1250, 2000
Fixed parameters		
Parameter	Values	
Workpiece	Cu, SS304, Ti grade 2	
Tool electrode	Tungsten 515 μm diameter	
Polarity	Tool (–), workpiece (+)	
Capacitance	10^4 pF	
Layer thickness	50 μm	
Length of cut	10^4 μm	
No. of layers	20 (10 to-and-fro layers each)	
Dielectric fluid	Hydrocarbon oil	

Besides the process parameters, the combination of tool and workpiece material also plays a major role in machinability performance of a μEDM process [20]. Typically, the wear resistance of tool electrode should be higher and must remove maximum material with minimum self-erosion [21]. Evaluation of surface morphology is also important as it plays a significant role in applicability of the products in several key engineering applications. The surface morphology is dependent on process parameters, type of dielectric and material properties (tool electrode and workpiece). D'Urso et al. [22] proposed a method of surface study by evaluating peaks and

Table 3 Taguchi L_9 orthogonal array and result of response measures

Exp. no.	Voltage (V)	Feed rate (μm/s)	Tool rotation speed (rpm)	MRR × 10^4 (μm^3/s)			TWR × 10^3 (μm^3/s)		
				Cu	SS	Ti	Cu	SS	Ti
1	80	5	500	6.12	3.73	4.44	2.23	4.55	3.38
2	80	12.5	1250	15.62	6.26	9.71	4.35	7.19	6.13
3	80	20	2000	28.72	11.80	15.21	7.85	11.74	10.99
4	130	5	1250	11.19	4.72	6.55	3.29	5.63	4.72
5	130	12.5	2000	23.57	9.68	11.58	6.90	10.26	9.33
6	130	20	500	31.00	11.45	16.02	8.61	11.22	10.00
7	180	5	2000	16.03	7.18	8.80	4.94	7.16	6.40
8	180	12.5	500	25.02	10.53	12.22	7.49	9.34	8.87
9	180	20	1250	38.06	17.03	18.42	11.31	15.01	13.81

valleys distribution, and shape after performing μED-milling on steel and ceramic materials. Properties like thermal diffusivity, boiling point, thermal conductivity and melting point play vital role in erosion by discrete sparks, which ultimately affect surface morphology of the material undergoing erosion by μEDM [23]. Feng et al. [24] found that specific heat and thermal conductivity played vital roles in the extent of weld pool depth due to spark. They observed surface morphology of Ti–6Al–4V to be of superior quality as compared to SUS316 and SKH59, due to the formation of shallow craters in Ti–6Al–4V. Higher specific heat capacity and lower thermal conductivity were accounted for the formation of shallow craters in Ti–6Al–4V.

From the literature, it can be inferred that μED-milling is still a new practice which is yet to be standardized for all engineering materials. Moreover, achieving a stable condition of μED-milling is a daunting task. Several electrical and non-electrical parameters play important role in achieving a stable μED-milling condition for a combination of tool electrode and workpiece material. In addition, electrical and thermal properties of the materials also play a significant part in determining the ease of machinability in μED-milling. In the present day, focus is mostly on micromachining of biomedical materials such as stainless steel, Ti and its corresponding alloys. The capability of μED-milling to fabricate complex microfeatures in any conductive material makes it obligatory to investigate machinability of such materials using μED-milling. An in-depth analysis regarding machinability study of Ti grade 2 and SS304 using μED-milling and study of their surface morphology is still lacking in the present scenario. It is also important to know their surface characteristics as surface performance will directly affect reliability of any component manufactured by μED-milling of these materials [25]. Thus, a comparative analysis of machinability on three different materials such as Cu, SS304 and Ti grade 2 using μED-milling is carried out in this study. The study also exhibits the prospect of μED-milling on different materials based on their electrical and thermal properties, which holds significant influence on the performance of any μEDM variant.

2 Materials and Methods

A tabletop-type μEDM machine setup (Model: Hyper 15, Make: Synergy Nano System, Mumbai, India) is used to conduct the experiments. Tungsten rod of 515 μm in diameter is used as tool electrode due to its higher electrical erosion resistance property [26]. Biocompatible materials such as SS304 and Ti grade 2 along with readily used Cu are taken as workpiece. Some of their physical properties which possess the potential to play significant role in μED-milling are enlisted in Table 1 [27–29].

Pilot experiments are conducted to ascertain the effective process parameters and their corresponding levels in establishing μED-milling process on the selected workpiece materials. By preliminary experimentation, it is observed that capacitance plays a decisive role in stabilizing the milling process. Significant inefficiency of μED-milling process is observed while lowering the capacitance value. So, capacitance is kept fixed at 10^4 pF throughout the final experimentation. It is also observed that negative polarity of tool electrode results in more removal of material from workpiece as compared to the positive polarity of tool. As a result, polarity is also kept fixed (tool: negative; workpiece: positive) throughout the experimentation. Hydrocarbon oil is used as dielectric medium, and jet flushing is applied to evacuate the debris from the machining zone. Substantial variation of machinability is observed with the change of voltage, FR and TRS without destabilizing the process. So voltage, FR and TRS are chosen as the process parameters for investigation. The experimental condition consisting of fixed and variable process parameters with their corresponding levels is depicted in Table 2. Based on the selected levels of process parameters, a Taguchi L_9 orthogonal array is formulated

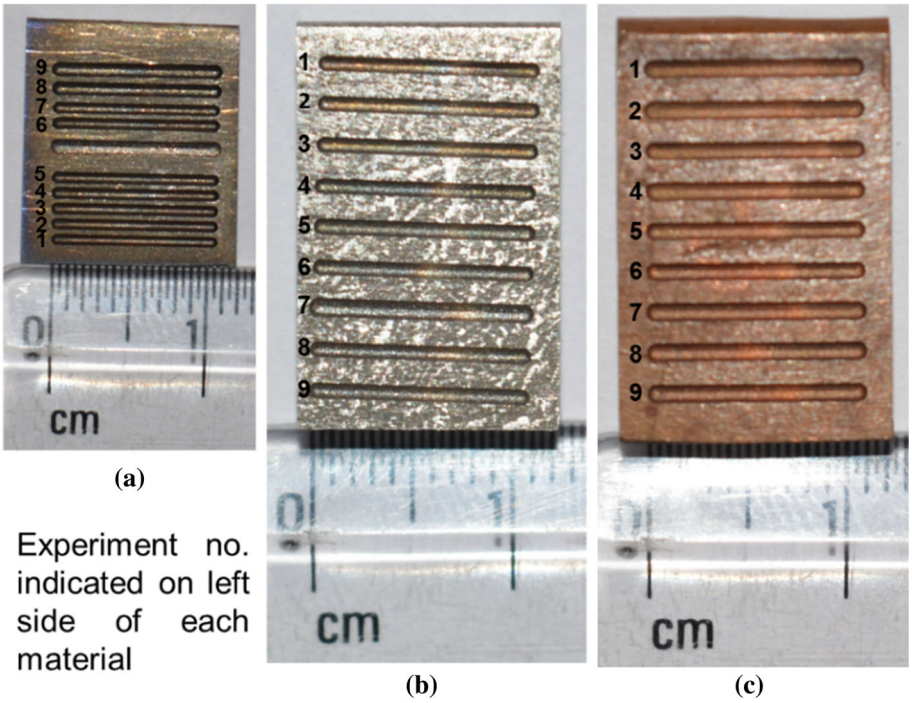

Fig. 1 Microchannels fabricated by μED-milling on **a** Ti grade 2, **b** SS304 and **c** Cu

and experiments are conducted based on the combination of process parameters as shown in Table 3.

Experiments are performed based on layer by layer machining strategy of μED-milling. Layer thickness (depth of cut) of 50 μm is applied in each 'to-and-fro' layer. The dimensional inaccuracy caused in machining one 'to' layer is neutralized by the subsequent machining of one 'fro' layer. Length of machining is kept sufficiently large at 10^4 μm, so that the tool tip is able to regain its original shape at the end of machining each 'to' or 'fro' layer. Thus, 'to-and-fro' motion of tool coupled with ample machining length of 10^4 μm compensates the dimensional inaccuracy caused by the tool wear in μED-milling.

The response parameters TWR and MRR are calculated by determining the volumetric removal of material from tool electrode and workpiece, respectively. Calculation of MRR is based on determining the average depth, average width of milling slot and machining time as given in Eq. (1). The depth of the milling slots is measured by electrical contact of the tool electrode on the slots with respect to a fixed reference point. The width of the slots is measured by optical microscopy. TWR is calculated by determining the radius of tool electrode, length of eroded tool and machining time, as given in Eq. (2). The eroded length of tool is also measured by electrical contact to a fixed point before and after machining. The microchannels fabricated by μED-milling process on the three workpieces: Ti grade 2, SS304 and Cu, are shown in Fig. 1.

$$\text{MRR} = \frac{\text{depth}_{\text{average}} \times \text{width}_{\text{average}} \times \text{length}}{\text{machining time}} \tag{1}$$

$$\text{TWR} = \frac{\pi r^2 \times h}{\text{machining time}} \tag{2}$$

where 'r' denotes radius of the tool electrode and 'h' denotes the eroded length.

3 Results and Discussion

3.1 Effect of Process Parameters

The results of MRR and TWR are depicted in Table 3. The voltage at which the current flows through the inter-electrode gap to initialize spark is called breakdown voltage. Mean effect plot to depict the effect of voltage on MRR of the three materials is shown in Fig. 2a. Irrespective of the different type of materials used, MRR increases with an increment in voltage in all the cases. The discharge energy for RC pulse circuit is the product of voltage (V) and capacitance (C) as expressed in Eq. (3) [30]:

$$\text{Discharge energy} = \frac{1}{2} C V^2 \tag{3}$$

As capacitance is kept constant at 10^4 pF throughout the experimentation, an increase in voltage leads to an increment in discharge energy of the process. With the increase in energy per discharge, the amount of charge released during discharge increases, subsequently resulting in more number of ions moving with higher velocity [13]. This leads to high pressure and temperature in plasma channel facilitating

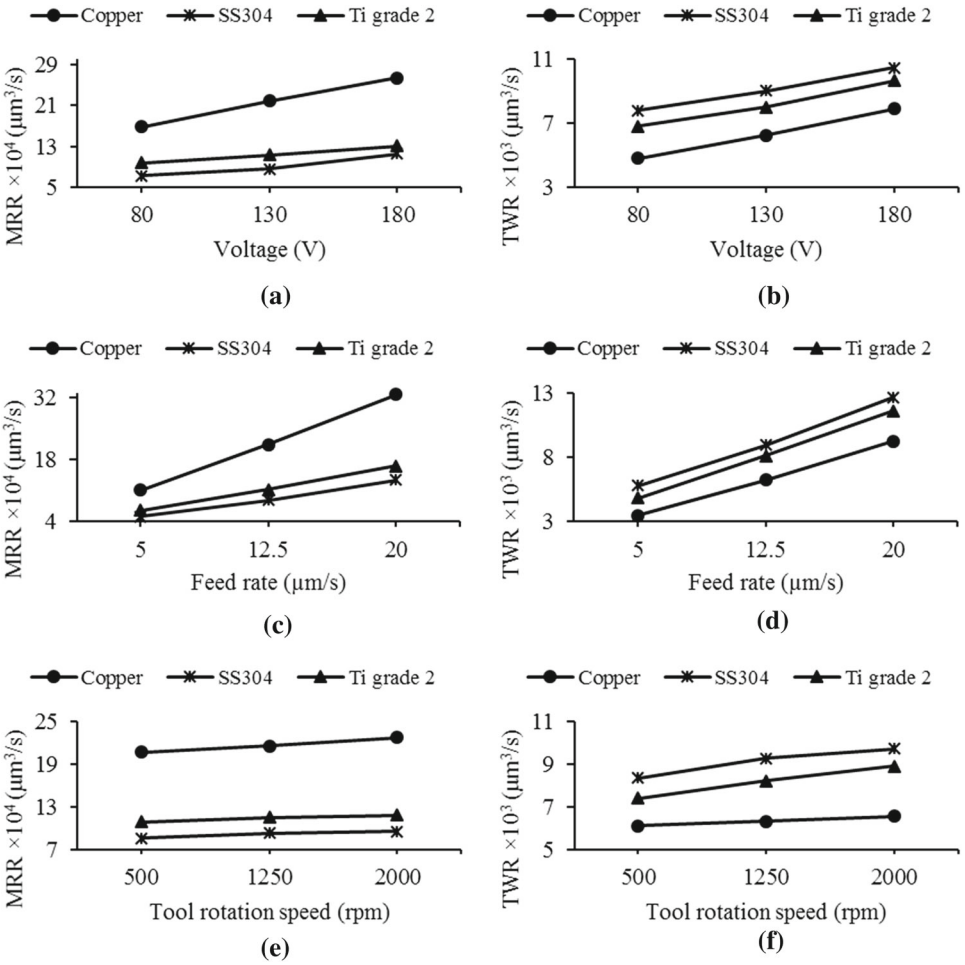

Fig. 2 Effect of **a** voltage on MRR, **b** voltage on TWR, **c** feed rate on MRR, **d** feed rate on TWR, **e** tool rotation speed on MRR and **f** tool rotation speed on TWR

higher MRR. The trend of MRR against voltage for all the materials is $MRR_{Cu} > MRR_{Ti} > MRR_{SS304}$.

Tool wear is inevitable in µED-milling process, which occurs primarily due to impingement of high-density electrons. Further, thermal effect and microstructural imperfections of the tool material also contribute to tool wear [31]. Mean effect plot to depict the effect of voltage on TWR is shown in Fig. 2b. Similar to MRR, an increase in voltage leads to higher TWR in all the materials due to the rise in discharge energy. The trend of TWR against voltage for all the materials is $TWR_{SS304} > TWR_{Ti} > TWR_{Cu}$.

FR in µED-milling regulates the time necessary for the tool electrode to maintain the inter-electrode gap after each consecutive discharge. Mean effect plot to depict the effect of FR on MRR of the three materials is shown in Fig. 2c. In all the three materials, MRR increases with an increase in FR. FR affects the total machining time as an increase in FR rises the speed of retraction and forward movement of the electrode after encountering a short circuit. Thus, a higher FR lessens the idle time or non-sparking time and consequently increases the MRR [32]. The trend of MRR against FR for all the materials is $MRR_{Cu} > MRR_{Ti} > MRR_{SS304}$.

Mean effect plot to depict the effect of FR on TWR is shown in Fig. 2d. In all the materials, it is observed that TWR increases with an increment in FR. With an increase in FR, the tool positions itself quickly with its closest point of the workpiece leading to faster electron emission from the tool electrode. Also, the debris get trapped as they do not get sufficient time to flush away, causing secondary spark with the tool leading to higher tool wear [1]. The trend of TWR against FR for all the materials is $TWR_{SS304} > TWR_{Ti} > TWR_{Cu}$.

Rotation of the tool electrode produces a centrifugal force and agitation effect which assist in regulating the dielectric fluid and flushing away of the debris from the machining zone [16, 33]. Mean effect plot to depict the effect of TRS on MRR of the three materials is shown in Fig. 2e. In each of the materials, MRR increases steadily with an increase in TRS. The spin stability imparted on tool by rotation prevents short circuiting by compensating force of shock wave and enhancing normal discharge [13]. With the increase in TRS, the number of normal discharge increases leading to higher MRR. The trend of MRR against TRS for all the materials is $MRR_{Cu} > MRR_{Ti} > MRR_{SS304}$.

Table 4 ANOVA of response measures

1. Copper						
1.1 Material removal rate (MRR)						
Source	DOF	Sum of square	Mean square	F ratio	p value	Contribution (%)
Voltage	2	137.141	68.571	31.45	0.031	16.32
FR	2	692.610	346.305	158.85	0.006	82.40
TRS	2	6.411	3.205	1.47	0.405	0.76
Error	2	4.360	2.180	–	–	0.52
Total	8	840.522	–	–	–	100
$R^2 = 99.48\%$, $R^2(\text{adj}) = 97.93\%$						
1.2 Tool wear rate (TWR)						
Voltage	2	14.4671	7.2336	12.75	0.073	21.95
FR	2	49.9954	24.9977	44.06	0.022	75.85
TRS	2	0.3156	0.1578	0.28	0.782	0.48
Error	2	1.1348	0.5674	–	–	1.72
Total	8	65.9129	–	–	–	100
$R^2 = 98.28\%$, $R^2(\text{adj}) = 93.11\%$						
2. Stainless steel 304						
2.1 Material removal rate (MRR)						
Voltage	2	29.214	14.6071	5.60	0.152	21.21
FR	2	101.681	50.8407	19.48	0.049	73.83
TRS	2	1.601	0.8006	0.31	0.765	1.16
Error	2	5.219	2.6095	–	–	3.80
Total	8	137.716	–	–	–	100
$R^2 = 96.21\%$, $R^2(\text{adj}) = 84.84\%$						
2.2 Tool wear rate (TWR)						
Voltage	2	10.794	5.397	3.35	0.230	12.27
FR	2	71.127	35.564	22.10	0.043	80.85
TRS	2	2.838	1.419	0.88	0.531	3.22
Error	2	3.218	1.609	–	–	3.66
Total	8	87.978	–	–	–	100
$R^2 = 96.34\%$, $R^2(\text{adj}) = 85.37\%$						
3. Titanium grade 2						
3.1 Material removal rate (MRR)						
Voltage	2	16.943	8.4717	280.52	0.004	10.13
FR	2	148.803	74.4015	2463.64	0.000	88.95
TRS	2	1.482	0.7411	24.54	0.039	0.88
Error	2	0.060	0.0302	–	–	0.04
Total	8	167.289	–	–	–	100
$R^2 = 99.96\%$, $R^2(\text{adj}) = 99.86\%$						

Table 4 continued

3.2 Tool wear rate (TWR)						
Voltage	2	12.387	6.194	4.68	0.176	14.24
FR	2	68.614	34.307	25.91	0.037	78.87
TRS	2	3.342	1.671	1.26	0.442	3.85
Error	2	2.649	1.324	–	–	3.04
Total	8	86.992	–	–	–	100
$R^2 = 96.96\%$, $R^2(\text{adj}) = 87.82\%$						

DOF degree of freedom

Mean effect plot to depict the effect of TRS on TWR is shown in Fig. 2f. TWR increases with an increase in TRS for all the materials due to improved flushing action at higher speed. Due to rotation, spark position keeps changing by not allowing the discharge energy to concentrate at a point and results in the formation of smaller-sized craters on the machined surface. An increase in speed can be correlated with an increase in frequency in a conventional circuit facilitating material removal from tool electrode [32]. The trend of TWR against TRS for all the materials is $TWR_{SS304} > TWR_{Ti} > TWR_{Cu}$.

The trend of the materials in descending order of MRR against all the process parameters is $MRR_{Cu} > MRR_{Ti} > MRR_{SS304}$. The thermal conductivity and electrical conductivity of Cu are far superior to SS304 and Ti grade 2. The higher electrical conductivity helps in quick initiation of spark in Cu as compared to SS304 and Ti grade 2. In traditional EDM, MRR decreases with an increase in thermal conductivity as heat dissipates faster with the increase in thermal conductivity of materials. Following this principle, Cu should have undergone lower wear than SS304 and Ti grade 2, but the use of very short nanopulses in μED-milling hinders the thermal conductivity to play any role as machining occurs rapidly within very short span of time. Elsewhere, the thermal conductivity of Ti grade 2 is almost similar to SS304 but MRR of Ti grade 2 is higher than SS304 in all the experiments. This trend can be attributed to a higher electrical conductivity of Ti grade 2, facilitating faster spark generation as compared to SS304. In case of TWR, the trend of the materials in descending order is $TWR_{SS304} > TWR_{Ti} > TWR_{Cu}$ against all the process parameters. The high melting point and positive polarity of tool electrode allow lower wear from tool as compared to the workpiece. The ease of spark formation in Cu with less short circuiting facilitates the traverse feed of the tool with less delay, leading to less tool wear. The difference of melting point temperature between workpiece and tool electrode also leads to easy erosion of workpiece with lower tool wear [34]. Thus, Cu workpiece bearing lower melting point as compared to SS304 and Ti grade 2 incurs lower TWR. The electrical conductivity of SS304 being lower than that of Ti grade 2 causes higher amount of delay in sparking (in SS304) and allows sufficient time for melting of tool material. Such higher delay in sparking leads to higher TWR in SS304 than Ti grade 2.

3.2 Analysis of Variance (ANOVA)

ANOVA is a statistical tool used to evaluate the significance of each process parameter in the response measures. The results of ANOVA for MRR and TWR are depicted in Table 4. In MRR and TWR models of all the materials, FR is the highest contributing factor followed by voltage and TRS. The contribution of error is lower than all the process parameters in most of the cases, with highest error of 3.80% occurring in MRR model of SS304 material. The errors can be attributed to the setup errors related to clamping of tool electrode and workpiece. The measurement error related to depth determination by electrical contact of tool electrode also contributes toward overall error. The MRR model of SS304 bears the lowest correlation coefficient (R^2) value of 96.21% and adjusted correlation coefficient (R^2(adj)) value of 84.84%, respectively. Such high R^2 and R^2(adj) values indicate better significance of the MRR and TWR models [35].

3.3 Confirmation Experiment

Confirmation test is performed at optimum parametric setting of response measures for all the materials. In case of TWR, the optimum setting of TWR for all the materials (voltage at 80 V, FR at 5 μm/s and TRS at 500 rpm) is included in the main experiment (experiment number 1). So, confirmation experiment is not required for TWR. In case of MRR, the optimum parametric combination of voltage at 180 V, FR at 20 μm/s and TRS at 2000 rpm is not included in main experiment. So, confirmation test for MRR is conducted for all the materials. The result of predicted and confirmation test at optimum condition of MRR is depicted in Table 5. Deviation of 1.31%, 4.62% and 1.18% is obtained between the confirmation experiment and predicted results of MRR in Cu, SS304 and Ti grade 2 alloy, respectively. Such low deviation

Table 5 Predicted and confirmation experiment result at optimum condition

Sr. no.	Material	Response	Optimum condition	Result		Deviation (%)
				Predicted	Experiment	
1	Cu	MRR $\times 10^4$ ($\mu m^3/s$)	Voltage 180 V; FR 20 μm/s; TRS 2000 rpm	38.3352	38.8456	1.31
2	SS304			16.2519	17.0398	4.62
3	Ti grade 2			18.6799	18.9023	1.18

justifies the applicability of Taguchi method in optimizing process parameters of μED-milling process.

3.4 Surface Characterization

3.4.1 Spheroidization and Globule Formation

In μED-milling, the discharge points change rapidly due to the simultaneous action of tool rotation and movement in lateral axis. The ejection speed and direction of molten material removed from the workpiece depend on TRS, dielectric flow rate and flushing direction [36]. The high surface tension and its characteristic nature to decrease surface energy along with quenching action of the dielectric medium lead to balling effect or spheroidization of the ejected molten materials [37, 38]. The spheroidization effect gives rise to the formation of non-crystalline spherical particles called globules. The formation of spheroids can also be attributed to the absence of oxides on particle surface as both the electrodes are submerged in liquid dielectric [13]. The molten material removed from the parent material forms granules of different sizes. Depending on the amount of gases released during discharge and nucleation point of cooling, the globules may be either solid or hollow. The SEM micrographs shown in Fig. 3 illustrate the spheroidization effect and formation of globules in different materials and their dependence on voltage, FR and TRS. During rotation, the spark gap changes constantly and the spark gets destroyed or dispersed before the completion of discharge. Such unsettled sparks result in the formation of shallow and elongated cavities. With an increase in TRS, the emitted particles eject out of the melt zone at higher speed due to superior stirring action of tool electrode. Such high-speed ejection splits the particle jet to form finer particles of random size. The dominance of this effect in all the materials (see Fig. 3) increases with an increase in TRS (500 rpm $<$ 1250 rpm $<$ 2000 rpm). Moreover, the globules are subjected to centrifugal and viscous forces imparted by rotation of the tool electrode. The viscous force disperses the globules from the tool by imparting angular velocity, whereas the centrifugal force drives them toward cold surface of the stationary workpiece. This phenomenon results in resolidification of ejected molten material in the cavity with pronounce effect on the vicinity of cavity edge. The combination of both forces crashes the globules into spherical patterns. With an increment in voltage, the discharge energy increases, which in turn produces more number of globules with a rise in their size. This phenomenon is evident from Fig. 3, wherein superior globule formation in case of all the materials is clearly depicted at the use of 180 V as compared to lower voltage of 130 V and 80 V. Similar observation was also reported by Unune and Mali [19] in fabricating microchannels on Inconel 718 using μED-milling.

Among all the materials, Ti grade 2 shows minimum spheroidization effect due to proper flushing away of the debris. As the specific heat capacity of Ti is higher than SS304 and Cu, highest discharge energy is required to melt Ti and the resultant weld pool is smallest among all the materials [24]. Furthermore, unlike Cu, lower thermal conductivity of Ti restricts transmission of the energy to surrounding parts of the workpiece. As a result, the discharge sparks cause less penetration in its surface and result in formation of shallow craters. The origination of these shallow craters facilitates easy flushing away of the debris with negligible globule formation. Furthermore, resolidified layer is observed in machined cavity of all the materials, with pronounce resolidification occurring at higher parametric condition of voltage, FR and TRS. To further illustrate the formation of globules and resolidification, the characteristics of crater at different parametric condition for all the three materials are analyzed in the subsequent subsection.

3.4.2 Crater Characteristics and Redeposition

In μED-milling, stirring action of rotated tool creates overlapping craters which lead to the formation of globules of varying sizes [13]. Occurrence of sparks in immediate succession and adjacent to one another is the principal factor responsible for the formation of overlapping craters. The spark gap between the electrodes at a particular point varies due to the incorporation of rotational motion of the tool. This variation in spark gap either disperses or breaks the spark prior to its complete discharge, resulting in formation of shallow and elongated craters. The resultant craters improve the surface finish of tool and workpiece which shows the usefulness of simultaneous sparking. Figure 4 shows the distribution of craters at different parametric conditions of μED-milling on Cu, SS304 and Ti grade 2 alloy. Size of the craters is mainly dependent on the discharge energy [39].

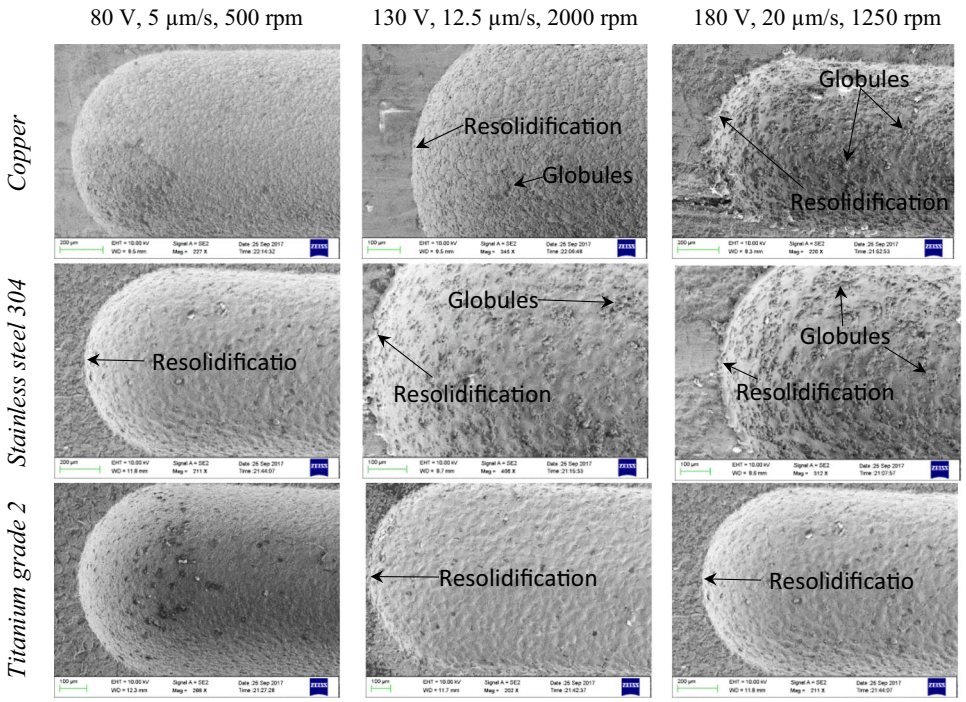

Fig. 3 SEM micrographs showing globule formation in machined cavity at different parametric condition of µED-milling

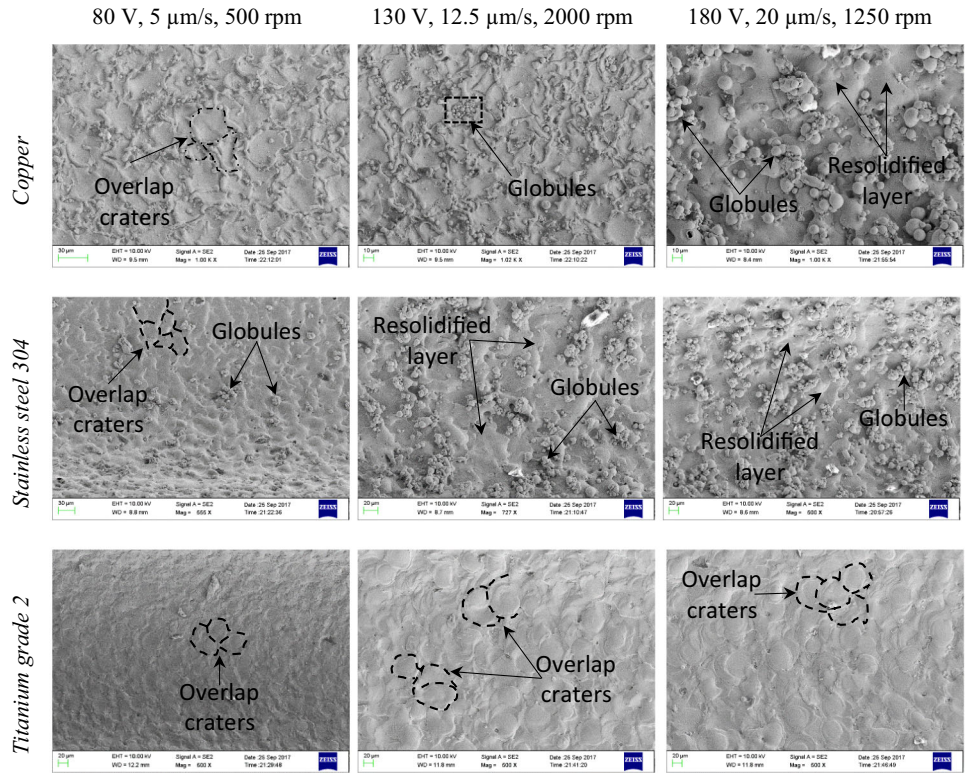

Fig. 4 Characteristics of crater at different parametric condition of µED-milling

With an increase in voltage, the crater sizes are seen to increase due to the discharge of higher energy. Similar finding has also been reported by Jahan et al. [40] while machining Ti–6Al–4V using µEDM. In Cu and SS304, the globule formation increases with an increment in voltage which can be attributed to partial/incomplete evaporation of molten material. During dispersion of one spark, rotation of tool can generate a successive new spark in close proximity of the previous spark, causing overlap of multiple sparks on same part of the workpiece. The overlapped craters form the source for bigger size globules by assimilating molten metal from the individual craters. But heavier assimilated pool of molten

metal often forms redeposition layer without forming globule. This phenomenon is visible in Cu and SS304, wherein more pronounced effect of globule formation is seen in case of machining with higher values of process parameters (see Fig. 4). On the contrary, Ti grade 2 shows overlapping craters but globule formation is minimum or negligible. This can be attributed to the formation of shallow craters in Ti grade 2 as compared to Cu and SS304, which facilitates easy flushing away of debris.

Moreover, globules resulting from crater are fragmented into random finer-sized particles by the stirring action of tool rotation. However, it is not effective in case of coarser globules as they require higher time for cooling than mixing, which consequently results in solidification to form redeposition layer. Thus, fragmentation and assimilation of molten metal are arbitrary processes that occur when tool rotation is employed as observed in Fig. 4. Redeposition is a general phenomenon occurring in EDM process due to the sudden cooling of molten materials. During μED-milling, molten materials are dispersed toward the edges of microchannel along the direction of rotation. Such flow of molten material for a certain distance results in a non-uniform solidification and thick layer of deposition at the microchannel edges as depicted in Fig. 3. The distance of molten material flow depends on its fluidity and TRS, wherein the fluidity depends on discharge energy and plasma temperature. Similar to overlapped craters, redeposition layer is also seen to overlap one another due to cooling of one molten layer over another with slender offset. The effect is pronounced at higher values of process parameters (voltage, FR and TRS) due to higher fluidity of molten material and cooling time. On the contrary, a less number of overlapped layers are observed at lower parametric values which signify the presence of less amount of molten material. Subsequently, the molten material (less amount) gets easily spread over the surface during cooling and yields better surface finish. To further apprehend the redeposition phenomenon in all the materials, an attempt has been made to investigate recast layer formed on the slots. For visualizing recast layer, cross section of the samples is first polished to attain mirror finish and then etched with suitable etchant as per the material's requirement. Figure 5 shows random cross-sectional micrograph of microslot machined at 130 V, 12.5 μm/s and 2000 rpm in three different materials. Among all the materials, Ti possesses lowest average layer thickness (7.71 μm) followed by and SS304 (14.05 μm) and Cu (21.31 μm). The higher recast layer thickness of Cu is due to its higher thermal conductivity (Table 1), which allows ease of heat transfer in Cu as compared to the other materials [25]. However, relatively lower thickness of recast layer in Ti as compared to SS304 can be attributed to formation of shallow craters in the former as the thermal conductivity of both the metals are almost similar. Overall, it has been found that although redeposition phenomenon and globule formation occur in all the materials, these are less dominant on Ti grade 2 as compared to SS304 and Cu.

3.4.3 Milling Marks and Microvoid Formation

Light milling marks are observed on the microchannels fabricated in each of the three materials (Cu, SS304 and Ti grade 2) as shown by curved lines in Fig. 6. These marks are not so prominent as compared to that of microchannels machined by conventional micromilling process. In case of each material taken in the present study, the milling marks shown in Fig. 6 are due to clockwise rotation of tool electrode and lateral feed of workpiece from right-hand side to left-hand side. μED-milling is performed by to-and-fro scanning method to achieve dimensional accuracy. But even this scanning method leaves some marks over the surface depicting the motion of tool and workpiece. To obtain surface devoid of any milling marks, some sort of post-processing technique must be applied on the microchannels. In addition to the milling marks, very few microvoids are observed to be scattered across the full length of microchannel in each of the three materials.

Arbitrary sample area of machined surface depicting microvoids in Cu, SS304 and Ti grade 2 alloy is shown in Fig. 6. Microvoids are generally formed due to the development of stress in the machined surface. In any EDM process, globules are generally formed due to partial/incomplete evaporation or recondensation of material. Recondensed material does not affect the integrity of machined surface, and very often, the stress concentration occurs in the site of partial/incomplete evaporation of material [41]. In the present study, a large number of microvoids are observed in Cu and SS304, which suggest formation of larger-sized globules and partial/incomplete evaporation of these two materials. In case of Ti grade 2, very less amount of microvoids combined with the formation of negligible amount of globules indicate that partial evaporation and recondensation have occurred fewer times than Cu and SS304. Thus, it can be concluded that Ti grade 2 alloy exhibits superior surface integrity as compared to Cu and SS304 in μED-milling.

3.4.4 Surface Roughness

Surface roughness (Ra), also known as center line average (CLA) or arithmetic average (AA), has been evaluated for the micromachined specimens by a non-contact 3D surface profilometer (Make: Taylor Hobson). Within a specific length, Ra is calculated by evaluating the arithmetic average value of the profile departure from the mean line [35]. Ra has been obtained at different locations of the microchannels, and their mean is taken as the final Ra for the present study. Figure 7a shows the Ra of L_9 experiments of all the materials considered in the study. 3D surface plot and Ra plot taken at random

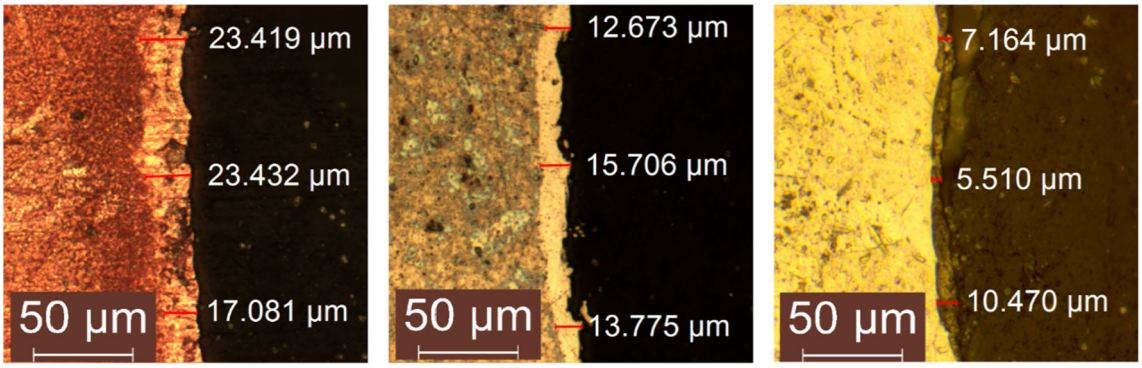

(a) Recast layer of Cu **(b)** Recast layer of SS304 **(c)** Recast layer of Ti grade 2

Fig. 5 Cross-sectional micrographs showing recast layer machined at 130 V, 12.5 µm/s and 2000 rpm. **a** Cu, **b** SS304 and **c** Ti grade 2

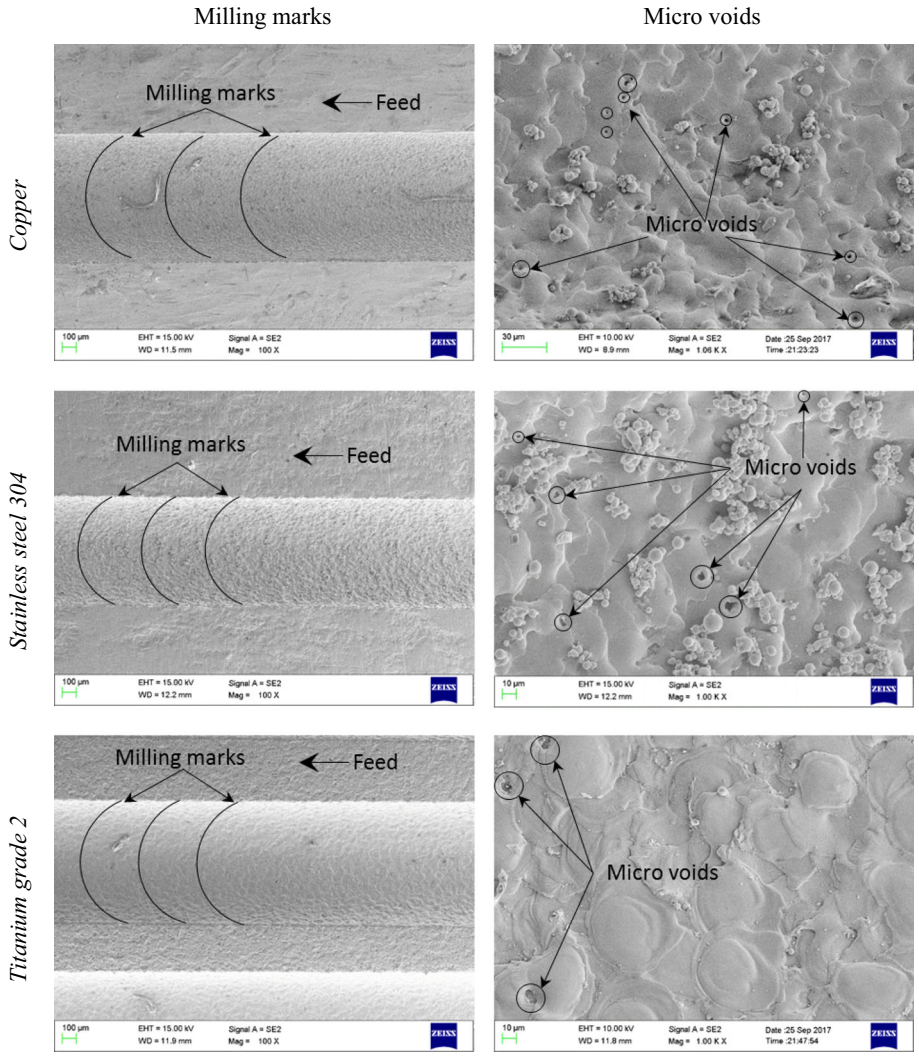

Fig. 6 Milling marks and microvoids formation in µED-milling of different materials

position of experiment performed at 130 V, 12.5 µm/s and 2000 rpm for Cu, SS304 and Ti grade 2 with their corresponding Ra values are shown in Fig. 8. The range of average Ra values is 1.18–1.89 µm for Cu, 1.19–4 µm for SS304 and 0.87–1.97 µm for Ti. The higher range of Ra in SS304 is due to non-uniform discharges leading to uneven distribution of craters. Mean effect plots depicting the effect of voltage, FR and TRS on Ra of the three materials are shown in Fig. 7b–d, respectively. With an increase in voltage, discharge energy increases, which leads to generation of craters of higher diam-

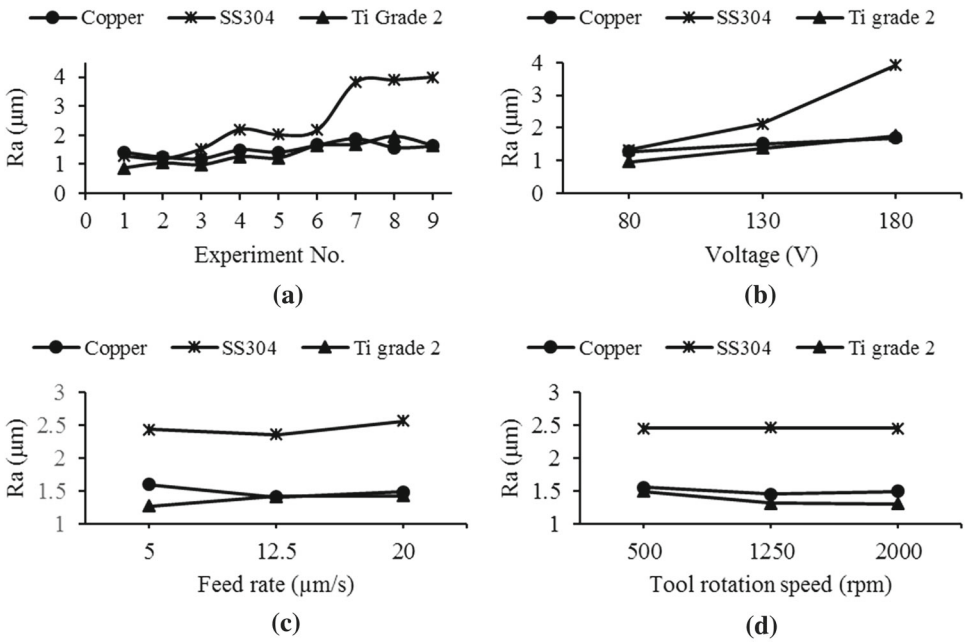

Fig. 7 **a** Surface roughness (Ra) of L_9 experiments, **b** effect of voltage on Ra, **c** effect of FR on Ra and **d** effect of TRS on Ra

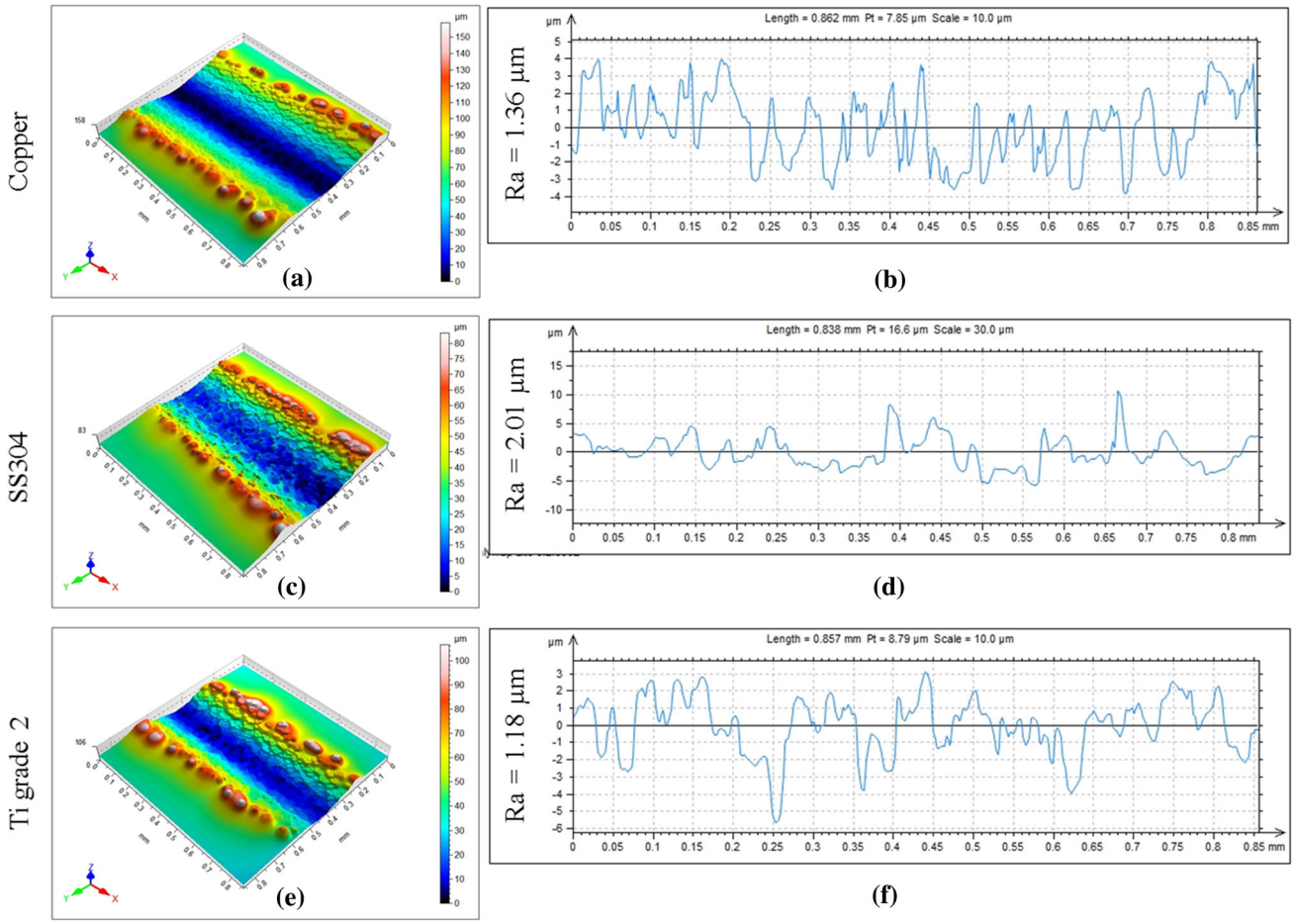

Fig. 8 Sample roughness plots at 130 V, 12.5 µm/s and 2000 rpm **a** 3D plot of copper, **b** Ra plot of copper, **c** 3D plot of SS304, **d** Ra plot of SS304, **e** 3D plot of Ti grade 2 and **f** Ra plot of Ti grade 2

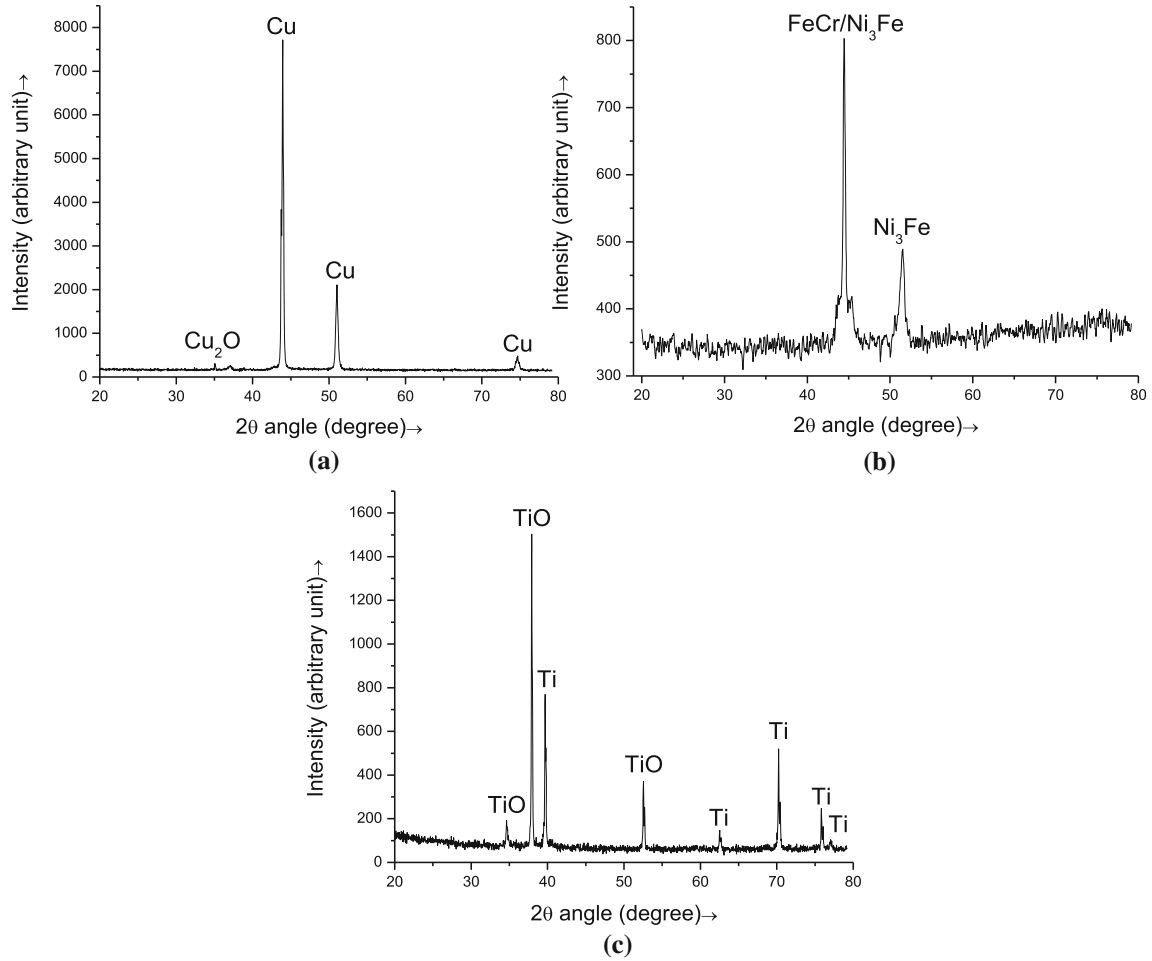

Fig. 9 XRD plot of **a** copper workpiece, **b** stainless steel 304 workpiece and **c** titanium grade 2 workpiece

eter [42]. This increase in crater diameter leads to an increase in Ra of all the materials. Ti exhibits lowest Ra in comparison to Cu and SS304 due to the formation of shallow craters [24]. Elsewhere, no particular trend has been observed for Ra against FR and TRS. Also, the effect of FR and TRS on Ra is relatively less as compared to that of voltage.

3.4.5 Material Composition Analysis

XRD analysis of the specimens is carried out to testify the composition of materials considered in the experiment as well as to determine the phases formed by μED-milling process. XRD plot of Cu, SS304 and Ti grade 2 machined with tungsten tool is shown in Fig. 9a–c, respectively. In case of Cu workpiece, traces of Cu_2O are found (see Fig. 9a) in XRD spectrum along with base material Cu. Traces of Ni_3Fe and FeCr are found in SS304 workpiece (see Fig. 9b), whereas traces of TiO along with base material Ti are found in Ti grade 2 alloy workpiece (see Fig. 9c). The material phases obtained by XRD analysis of the three samples after μED-milling process validate the properties of the undertaken materials considered in the present experimental work.

EDX analysis is done to find the material composition of microchannels and investigate whether there is any transfer of foreign material in the machined cavities. The spectrum analysis is conducted for two cases: one in the vicinity of the edge and the other on a random surface far from edge. Figure 10 shows the EDX spectrum taken in vicinity of the edge and on the random surface, and their corresponding EDX plots with contribution of weight% and atomic % of elements. In μED-milling with hydrocarbon oil as dielectric medium, the carbon atoms dissociate from dielectric medium due to the flow of energy. The presence of carbon is observed on edge vicinity of Ti grade 2 and Cu amounting to 12.95 and 24.74 weight%, respectively. Such higher weight% of carbon can be attributed to redeposition of molten material [13]. A good amount of tungsten (25.48 wt%) is found on the edge of SS304 indicating transfer of tool material. Elsewhere, in Cu and Ti grade 2, tool material is not found in both edge and random surface.

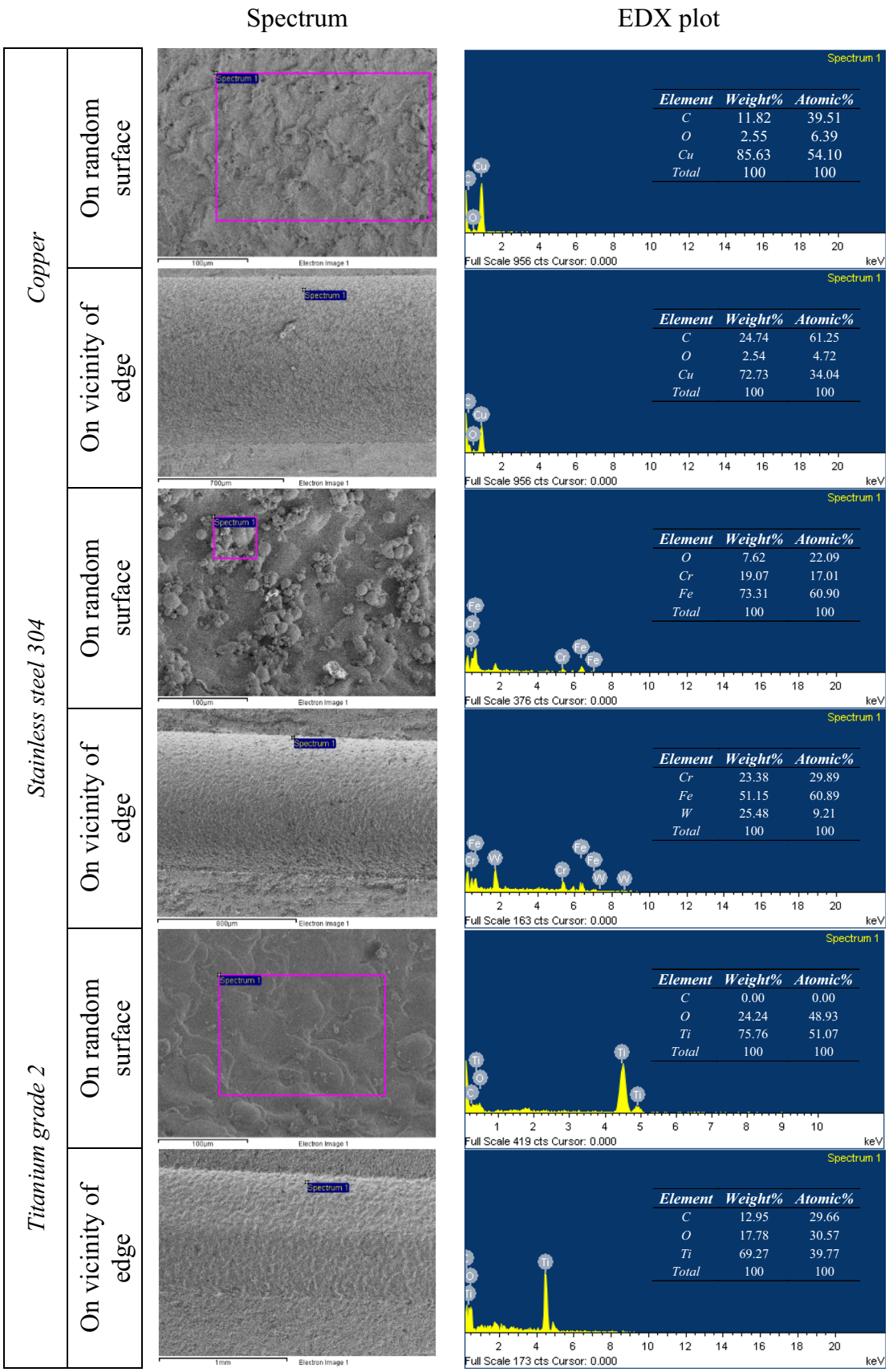

Fig. 10 EDX analysis of machined samples on edge and random surface

4 Conclusions

μED-milling has been successfully performed on Cu, SS304 and Ti grade 2 alloy. To-and-fro scanning method was utilized to negate the dimensional inaccuracies caused by tool wear. The following conclusions are drawn from the experimentation:

- MRR of Cu, SS304 and Ti grade 2 alloy increased with an increase in voltage, FR and TRS. Cu exhibited highest MRR followed by Ti grade 2 and SS304 at each parametric condition.
- An increment in voltage, FR and TRS led to an increase in the TWR of Cu, SS304 and Ti grade 2 alloy. SS304 exhibited highest TWR followed by Ti grade 2 and Cu.
- From ANOVA analysis, FR evolved as the most influential process parameter for both MRR and TWR, followed by voltage and TRS.
- Low deviation of 1.31%, 4.62% and 1.18% was observed between confirmation test and predicted result at optimum condition of MRR for Cu, SS304 and Ti grade 2 alloy, respectively.
- XRD analysis depicted that the material phases and elements pertain with the considered materials of this study. EDX analysis depicted higher weight% of carbon on the edge vicinity of Cu and Ti grade 2. Elsewhere, the presence of tungsten found on the edge vicinity of SS304 depicted transfer of tool material to the workpiece.
- Ti grade 2 exhibited better surface morphology as compared to SS304 and Cu, in terms of lower redeposition phenomenon, globule formation, stress concentration and Ra. This can be attributed to effective flushing away of debris due to the formation of shallow craters in μED-milling of Ti grade 2.

Acknowledgements The authors are thankful to CRF, National Institute of Technology Agartala; Production Engineering Department, National Institute of Technology, Agartala; and Ad-Nano Technologies, Bangalore, and Ishitv Technologies, Bangalore, to carry out characterization of the samples.

References

1. Mehfuz, R.; Ali, M.Y.: Investigation of machining parameters for the multiple-response optimization of micro electrodischarge milling. Int. J. Adv. Manuf. Technol. **43**, 264–275 (2009). https://doi.org/10.1007/s00170-008-1705-0
2. Prakash, V.; Kumar, P.; Singh, P.; Hussain, M.; Das, A.; Chattopadhyaya, S.: Micro-electrical discharge machining of difficult-to-machine materials: a review. Proc. Inst. Mech. Eng. B J. Eng. Manuf. **233**, 339–370 (2019). https://doi.org/10.1177/0954405417718591
3. Singh, A.K.; Patowari, P.K.; Deshpande, N.V.: Experimental analysis of reverse micro-EDM for machining microtool. Mater. Manuf. Process. **31**, 530–540 (2016). https://doi.org/10.1080/10426914.2015.1070426
4. Singh, A.K.; Patowari, P.K.; Deshpande, N.V.: Effect of tool wear on microrods fabrication using reverse μEDM. Mater. Manuf. Process. **32**, 1–8 (2017). https://doi.org/10.1080/10426914.2016.1198015
5. Wang, J.; Qian, J.; Ferraris, E.; Reynaerts, D.: In-situ process monitoring and adaptive control for precision micro-EDM cavity milling. Precis. Eng. **47**, 261–275 (2017). https://doi.org/10.1016/j.precisioneng.2016.09.001
6. Zhang, L.; Du, J.; Zhuang, X.; Wang, Z.; Pei, J.: Geometric prediction of conic tool in micro-EDM milling with fix-length compensation using simulation. Int. J. Mach. Tools Manuf. **89**, 86–94 (2015). https://doi.org/10.1016/j.ijmachtools.2014.11.007
7. Schulze, V.; Weber, P.; Ruhs, C.: Increase of process reliability in the micro-machining processes EDM-milling and laser ablation using on-machine sensors. J. Mater. Process. Technol. **212**, 625–632 (2012). https://doi.org/10.1016/j.jmatprotec.2011.09.014
8. Modica, F.; Basile, V.; Marrocco, V.; Fassi, I.: A new process combining micro-electro-discharge-machining milling and sinking for fast fabrication of microchannels with draft angle. J. Micro Nano-Manuf. **4**, 24501 (2016). https://doi.org/10.1115/1.4032324
9. Narasimhan, J.; Yu, Z.; Rajurkar, K.P.: Tool wear compensation and path generation in micro and macro EDM. J. Manuf. Process. **7**, 75–82 (2005). https://doi.org/10.1016/S1526-6125(05)70084-0
10. Kar, S.; Patowari, P.K.: Electrode wear phenomenon and its compensation in micro electrical discharge milling: a review. Mater. Manuf. Process. **33**, 1491–1517 (2018). https://doi.org/10.1080/10426914.2018.1453144
11. Mujumdar, S.S.; Curreli, D.; Kapoor, S.G.; Ruzic, D.: Modeling of melt-pool formation and material removal in microelectrodischarge machining. J. Manuf. Sci. Eng. **137**, 31007 (2015). https://doi.org/10.1115/1.4029446
12. Yang, F.; Qian, J.; Wang, J.; Reynaerts, D.: Simulation and experimental analysis of alternating-current phenomenon in micro-EDM with a RC-type generator. J. Mater. Process. Technol. **255**, 865–875 (2018). https://doi.org/10.1016/j.jmatprotec.2018.01.031
13. Karthikeyan, G.; Garg, A.K.; Ramkumar, J.; Dhamodaran, S.: A microscopic investigation of machining behavior in μED-milling process. J. Manuf. Process. **14**, 297–306 (2012). https://doi.org/10.1016/j.jmapro.2012.01.003
14. Karthikeyan, G.; Ramkumar, J.; Aravindan, S.: Performance analysis of μED-milling process using various statistical techniques. Int. J. Mach. Mach. Mater. **11**, 183 (2012). https://doi.org/10.1504/IJMMM.2012.045984
15. Chiou, A.-H.; Tsao, C.-C.; Hsu, C.-Y.: A study of the machining characteristics of micro EDM milling and its improvement by electrode coating. Int. J. Adv. Manuf. Technol. **78**, 1857–1864 (2015). https://doi.org/10.1007/s00170-014-6778-3
16. Kuriachen, B.; Mathew, J.: Experimental investigations into the effects of microelectric-discharge milling process parameters on processing Ti–6Al–4V. Mater. Manuf. Process. **30**, 983–990 (2015). https://doi.org/10.1080/10426914.2014.984206
17. Kuriachen, B.; Mathew, J.: Effect of powder mixed dielectric on material removal and surface modification in microelectric discharge machining of Ti–6Al–4V. Mater. Manuf. Process. **31**, 439–446 (2016). https://doi.org/10.1080/10426914.2015.1004705
18. Jafferson, J.M.; Hariharan, P.; Ram Kumar, J.: Effect of non-electrical parameters in μED milling: an experimental investigation. Int. J. Adv. Manuf. Technol. **85**, 2037–2047 (2016). https://doi.org/10.1007/s00170-015-7933-1
19. Unune, D.R.; Mali, H.S.: Experimental investigation on low-frequency vibration-assisted μ-ED milling of Inconel 718. Mater. Manuf. Process. **33**, 964–976 (2017). https://doi.org/10.1080/10426914.2017.1388516

20. D'Urso, G.; Ravasio, C.: Material-technology index to evaluate micro-EDM drilling process. J. Manuf. Process. **26**, 13–21 (2017). https://doi.org/10.1016/J.JMAPRO.2017.01.003
21. Samuel, M.P.; Philip, P.K.: Power metallurgy tool electrodes for electrical discharge machining. Int. J. Mach. Tools Manuf. **37**, 1625–1633 (1997). https://doi.org/10.1016/S0890-6955(97)00006-0
22. D'Urso, G.; Giardini, C.; Quarto, M.: Characterization of surfaces obtained by micro-EDM milling on steel and ceramic components. Int. J. Adv. Manuf. Technol. **97**, 1–9 (2018). https://doi.org/10.1007/s00170-018-1962-5
23. Tsai, Y.Y.; Masuzawa, T.: An index to evaluate the wear resistance of the electrode in micro-EDM. J. Mater. Process. Technol. **149**, 304–309 (2004). https://doi.org/10.1016/j.jmatprotec.2004.02.043
24. Feng, W.; Chu, X.; Hong, Y.; Zhang, L.: Studies on the surface of high-performance alloys machined by micro-EDM. Mater. Manuf. Process. **33**, 616–625 (2018). https://doi.org/10.1080/10426914.2017.1364758
25. Feng, W.; Chu, X.; Hong, Y.; Wang, K.; Zhang, L.: Studies on micro-EDM surface performance using a comprehensive method. Int. J. Adv. Manuf. Technol. **96**, 1875–1889 (2018). https://doi.org/10.1007/s00170-018-1711-9
26. Liu, W.; Jia, Z.; Zou, S.; Zheng, X.: A new measurement method of relative volume wear ratio based on discharge debris composition analysis in micro-EDM. Adv. Mech. Eng. **6**, 479609 (2014). https://doi.org/10.1155/2014/479609
27. Copper, Cu; Annealed, http://www.matweb.com/search/DataSheet.aspx?MatGUID=9aebe83845c04c1db5126fada6f76f7e
28. Stainless Steel, http://www.matweb.com/search/DataSheet.aspx?MatGUID=abc4415b0f8b490387e3c922237098da
29. Titanium Grade 2, http://www.matweb.com/search/datasheet.aspx?MatGUID=24293fd5831941ec9fa01dce994973c7&ckck=1
30. Jahan, M.P.; Wong, Y.S.; Rahman, M.: A study on the quality micro-hole machining of tungsten carbide by micro-EDM process using transistor and RC-type pulse generator. J. Mater. Process. Technol. **209**, 1706–1716 (2009). https://doi.org/10.1016/j.jmatprotec.2008.04.029
31. Singh, S.; Maheshwari, S.; Pandey, P.C.: Some investigations into the electric discharge machining of hardened tool steel using different electrode materials. J. Mater. Process. Technol. **149**, 272–277 (2004). https://doi.org/10.1016/j.jmatprotec.2003.11.046
32. Karthikeyan, G.; Ramkumar, J.; Dhamodaran, S.; Aravindan, S.: Micro electric discharge milling process performance: an experimental investigation. Int. J. Mach. Tools Manuf. **50**, 718–727 (2010). https://doi.org/10.1016/j.ijmachtools.2010.04.007
33. Mullya, S.; Karthikeyan, G.: Dielectric flow observation at inter-electrode gap in micro-electro-discharge-milling process. Proc. Inst. Mech. Eng. B J. Eng. Manuf. **232**, 1079–1089 (2016). https://doi.org/10.1177/0954405416662082
34. Moses, M.D.; Jahan, M.P.: Micro-EDM machinability of difficult-to-cut Ti–6Al–4V against soft brass. Int. J. Adv. Manuf. Technol. **81**, 1345–1361 (2015). https://doi.org/10.1007/s00170-015-7306-9
35. Kar, S.; Chakraborty, S.; Dey, V.; Ghosh, S.K.: Optimization of surface roughness parameters of Al-6351 alloy in EDC process: a taguchi coupled fuzzy logic approach. J. Inst. Eng. Ser. C **98**, 607–618 (2017). https://doi.org/10.1007/s40032-016-0297-y
36. Vidya, S.; Barman, S.; Chebolu, A.; Nagahanumaiah,; Das, A.K.: Effects of different cavity geometries on machining performance in micro-electrical discharge milling. J. Micro Nano-Manuf. **3**, 11007 (2015). https://doi.org/10.1115/1.4029275
37. Khanra, A.K.; Pathak, L.C.; Godkhindi, M.M.: Microanalysis of debris formed during electrical discharge machining (EDM). J. Mater. Sci. **42**, 872–877 (2007). https://doi.org/10.1007/s10853-006-0020-0
38. Kou, Z.; Han, F.: Machining characteristics and removal mechanisms of moving electric arcs in high-speed EDM milling. J. Manuf. Process. **32**, 676–684 (2018). https://doi.org/10.1016/J.JMAPRO.2018.03.037
39. Benavides, G.L.; Bieg, L.F.; Saavedra, M.P.; Bryce, E.A.: High aspect ratio meso-scale parts enabled by wire micro-EDM. Microsyst. Technol. **8**, 395–401 (2002). https://doi.org/10.1007/s00542-002-0190-x
40. Jahan, M.P.; Alavi, F.; Kirwin, R.; Mahbub, R.: Micro-EDM induced surface modification of titanium alloy for biocompatibility. Int. J. Mach. Mach. Mater. **20**, 274–298 (2018). https://doi.org/10.1504/IJMMM.2018.093548
41. Arooj, S.; Shah, M.; Sadiq, S.; Jaffery, S.H.I.; Khushnood, S.: Effect of current in the EDM machining of aluminum 6061 T6 and its effect on the surface morphology. Arab. J. Sci. Eng. **39**, 4187–4199 (2014). https://doi.org/10.1007/s13369-014-1020-z
42. Koyano, T.; Sugata, Y.; Hosokawa, A.; Furumoto, T.: Micro electrical discharge machining using high electric resistance electrodes. Precis. Eng. **47**, 480–486 (2017). https://doi.org/10.1016/J.PRECISIONENG.2016.10.003